Fractal Structure of Spin Clusters and Domain Walls in two-dimensional Ising Model

Wolfhard Janke and Adriaan M. J. Schakel

Institut für Theoretische Physik, Universität Leipzig, Augustusplatz 10/11, 04109 Leipzig, Germany

(Dated: June 11, 2018)

The fractal structure of spin clusters and their boundaries in the critical two-dimensional Ising model is investigated numerically. The fractal dimensions of these geometrical objects are estimated by means of Monte Carlo simulations on relatively small lattices through standard finite-size scaling. The obtained results are in excellent agreement with theoretical predictions and partly provide significant improvements in precision over existing numerical estimates.

I.   INTRODUCTION

The past few years have witnessed a surge in the geometrical approach to phase transitions. The prototype of such an approach is percolation theory [1], which focuses on clusters of (randomly) occupied sites or bonds on a lattice. The fractal structure of these geometrical objects and whether or not a cluster percolates the lattice are central topics addressed by the theory. Spin models such as the q-state Potts models can easily be mapped onto percolation theory, with neighboring spins in the same spin state lumped together in a cluster. Generally, the geometrical spin clusters thus constructed do not percolate at the critical temperature T_c where the thermal phase transition takes place. But by erasing with a certain temperature-dependent probability bonds between like spins, Fortuin and Kasteleyn (FK) [2] showed that spin clusters can be constructed for the Potts models that do percolate at T_c and encode the thermal critical behavior. They thus achieved a geometrical description of the thermal phase transition in these models. The cluster approach has been turned into an efficient Monte Carlo algorithm by Swendsen and Wang [3], and by Wolff [4], where not individual spins are updated, as in local spin updates with, e.g., the Metropolis algorithm, but entire FK clusters.

An exception to the rule that geometrical clusters do not percolate at T_c is the two-dimensional (2D) q-state Potts model. The origin of this effect can be understood by extending the pure lattice model to include vacant sites. In a Kadanoff block-spin approach, such an extension is natural as the vacant sites represent disordered blocks without a majority in any of the spin states, and is essential for establishing that the phase transition of the pure models changes from being continuous to first order at $q = 4$ [5, 6]. In addition to the pure Potts critical behavior, the site diluted model also displays tricritical behavior at the same critical temperature T_c. While the critical behavior of the pure model is encoded in the FK clusters, the tricritical behavior is encoded in the geometrical clusters [7, 8, 9]. Both cluster types percolate at T_c. With increasing q, the critical and tricritical fixed points, which are characterized by the same central charge c, move together until merging at $q = 4$.

Very recently, cluster boundaries of critical 2D systems have been studied analytically by means of the so-called stochastic Loewner evolution, introduced by Schramm [10]. Various exact predictions for critical exponents previously conjectured on the basis of the Coulomb-gas map [11, 12, 13] and conformal invariance [14] could rigorously be established by this method (for an overview see Ref. [15]).

In this paper, we numerically investigate the fractal structure of clusters in the 2D Ising model, corresponding to setting $q = 2$. We simulate the model on relatively small lattices ($L = 8 - 512$) with periodic boundary conditions, and apply standard finite-size scaling to determine the various fractal dimensions. In addition to studying the size or "mass" of FK and geometrical clusters, we also examine their boundaries. Those of geometrical clusters form the famous Peierls domain walls [16], separating spin clusters of opposite orientation. In a previous paper [9], we simulated these domain walls directly by considering the high-temperature representation of the model. By duality, the high-temperature graphs, which are closed, are domain walls on the dual lattice. The closed graph configurations were generated by means of a Metropolis update algorithm, involving single plaquettes.

Other recent numerical studies of the geometrical structure of 2D Potts models were reported in Refs. [17, 18]. Our results for the fractal dimensions are in excellent agreement with theoretical predictions [7, 13, 19, 20, 21], and provide in particular for the FK and geometrical clusters a considerable improvement in precision over the estimates obtained in Refs. [17, 18].

The rest of the paper is structured as follows. The next section summarizes the necessary theoretical background. Numerical results are presented in Sec. III, followed by concluding remarks in Sec. IV.

II.   FRACTAL STRUCTURES

The fractal properties of spin clusters and boundaries, which are clusters themselves, are described by a straightforward extension of ordinary percolation theory [1]. Asymptotically, cluster distributions ℓ_n take a general form

$$\ell_n \sim n^{-\tau} \exp(-\theta n), \tag{1}$$

consisting of two factors: (i) an entropy factor, which measures the number of ways a cluster of size n can be

embedded in the lattice, and (ii) a Boltzmann weight, which suppresses large clusters when θ is finite. Clusters proliferate and percolate the lattice when θ tends to zero. The vanishing is characterized by an exponent σ as $\theta \propto |T - T_{\mathrm{p}}|^{1/\sigma}$, where T_{p} denotes the percolation temperature. As explained in the Introduction, the percolation thresholds of both FK and geometrical clusters coincide with the thermal critical temperature of the 2D Ising model. The entropy exponent τ determines the fractal structure of the geometrical objects. Rather than extracting this exponent directly from the asymptotic behavior of a distribution at the percolation threshold, where the distribution becomes algebraic, it is expedient to extract it from derived quantities such as the percolation strength P_∞, giving the fraction of sites in the largest cluster, and the average cluster size [1]

$$\chi = \frac{\sum_n n^2 \ell_n}{\sum_n n \ell_n}. \tag{2}$$

Since every site belongs to some geometrical and some FK cluster, the denominator in Eq. (2) adds up to the total number of sites for these clusters. Close to the percolation threshold, the observables obey the finite-size scaling laws [22]

$$P_\infty = L^{-\beta/\nu}\, \mathsf{P}(L/\xi), \quad \chi = L^{\gamma/\nu}\, \mathsf{X}(L/\xi), \tag{3}$$

where L is the lattice size and ξ the correlation length whose divergence at criticality is governed by the exponent ν. The ratios β/ν and γ/ν are given in terms of τ as [1]

$$\frac{\beta}{\nu} = d\frac{\tau - 2}{\tau - 1}, \quad \frac{\gamma}{\nu} = d\frac{3 - \tau}{\tau - 1}, \tag{4}$$

with d the dimensionality of the lattice. The fractal dimension D, which is also determined solely by the entropy exponent τ, is related to these exponents via [1]

$$D = \frac{d}{\tau - 1} = d - \frac{\beta}{\nu} = \frac{1}{2}\left(d + \frac{\gamma}{\nu}\right). \tag{5}$$

Generically, two (and only two) different cluster boundaries can be identified [23]: the hull (H) and the external perimeter (EP), where the second can be understood as a smoother version of the first. For 2D FK clusters, the two boundaries are in one-to-one correspondence, with their fractal dimensions satisfying the relation [21]

$$(D_{\mathrm{H}}^{\mathrm{FK}} - 1)(D_{\mathrm{EP}}^{\mathrm{FK}} - 1) = \tfrac{1}{4}. \tag{6}$$

The map transforming one FK boundary dimension into the other conserves the central charge c, which may be parametrized as [12, 14]

$$c = 1 - \frac{6(1 - \bar{\kappa})^2}{\bar{\kappa}} = 13 - 6\left(\bar{\kappa} + \frac{1}{\bar{\kappa}}\right), \tag{7}$$

where $2 \geq \bar{\kappa} \geq 1$ parametrizes the two-dimensional q-state Potts models

$$\sqrt{q} = -2\,\cos(\pi/\bar{\kappa}), \tag{8}$$

with $0 \leq q \leq 4$. In terms of $\bar{\kappa}$, the fractal dimensions of the FK boundaries [13, 21] can be expressed as

$$D_{\mathrm{H}}^{\mathrm{FK}} = 1 + \frac{\bar{\kappa}}{2}, \quad D_{\mathrm{EP}}^{\mathrm{FK}} = 1 + \frac{1}{2\bar{\kappa}}, \tag{9}$$

while the central charge conserving map corresponds to letting $\bar{\kappa} \to 1/\bar{\kappa}$. These explicit forms are seen to satisfy the duality relation (6). With the scaling relations (5), the critical exponent ratios characterizing the FK boundaries become

$$\gamma_{\mathrm{H}}^{\mathrm{FK}}/\nu = \bar{\kappa}, \quad \gamma_{\mathrm{EP}}^{\mathrm{FK}}/\nu = 1/\bar{\kappa}, \tag{10}$$

where a single correlation length with exponent ν is assumed. It thus follows that the two FK boundary sizes scale with inverse exponents:

$$\chi_{\mathrm{H}}^{\mathrm{FK}} \sim L^{\bar{\kappa}}, \quad \chi_{\mathrm{EP}}^{\mathrm{FK}} \sim L^{1/\bar{\kappa}}. \tag{11}$$

In contrast to FK clusters, geometrical clusters are characterized by only one boundary dimension, i.e., the fractal dimensions $D_{\mathrm{H}}^{\mathrm{G}}$ and $D_{\mathrm{EP}}^{\mathrm{G}}$ of the hull and external perimeter coincide, $D_{\mathrm{H}}^{\mathrm{G}} = D_{\mathrm{EP}}^{\mathrm{G}}$. Such cases are signaled by a negative fractal dimension of the red sites [19], sites that, when removed, lead to a splitting of the cluster into disconnected parts.

The central charge conserving map $\bar{\kappa} \to 1/\bar{\kappa}$ transforming the hull dimension $D_{\mathrm{H}}^{\mathrm{FK}}$ of FK clusters into that of their external perimeters, $D_{\mathrm{EP}}^{\mathrm{FK}}$, also maps it onto the hull dimension of geometrical clusters, implying [21]

$$D_{\mathrm{EP}}^{\mathrm{FK}} = D_{\mathrm{H}}^{\mathrm{G}}. \tag{12}$$

This relation is remarkable as it involves the two different boundary types. In the context of uncorrelated percolation [23], the hull of a cluster in 2D is traced out by a directed random walker constrained to move on the cluster only, whereas the external perimeter is traced out by a walker constrained to move around the hull on sites neighboring, but not belonging to, that cluster.

To numerically verify relation (12), we wish to treat external perimeters of FK clusters and hulls of geometrical clusters in the same manner. To this end we apply the same algorithm used to trace out geometrical hulls to find the FK external perimeters, where it is recalled that FK clusters differ from geometrical clusters in that with a prescribed temperature-dependent probability bonds are erased. The difference between tracing out FK hulls and external perimeters then reduces to (see Fig. 1) allowing the random walker to move to a nearest neighbor site on the FK boundary only provided the connecting bond is set (hull) or always (external perimeter).

To conclude this section we list in Table I the predicted exact values [7, 13, 19, 20, 21] for the various fractal dimensions and corresponding critical exponents we wish to determine numerically.
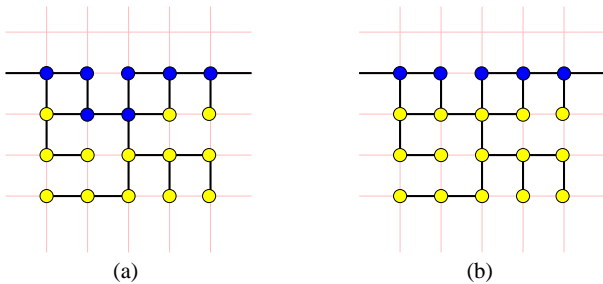
FIG. 1: (Color online) Part of a single FK cluster of nearest neighbor sites (filled circles) connected by bonds (black links). (a) Sites belonging to the hull (dark filled circles) are found by allowing the random walker tracing out the boundary to move only over set bonds. (b) Sites belonging to the external perimeter (dark filled circles) are found by allowing the random walker to move to a nearest neighbor on the cluster irrespective of whether the connecting bond is set or not. The external perimeter, which contains two sites less than the hull for this boundary segment, is therefore a smoother version of the hull.

	D_C	γ_C/ν	β_C/ν	D_H	γ_H/ν	D_{EP}	γ_{EP}/ν
FK	15/8	7/4	1/8	5/3	4/3	11/8	3/4
G	187/96	91/48	5/96	11/8	3/4		

TABLE I: Predicted values for the fractal dimensions with the corresponding critical exponents characterizing Fortuin-Kasteleyn (FK) and geometrical (G) clusters (C), their hulls (H), and external perimeters (EP).

III. MONTE CARLO SIMULATIONS

The simulation data was collected on square lattices of linear size $L = 8, 10, 12, 14, 16, 20, 24, 32, 40, 48, 64, 90,$ $128, 180, 256, 360,$ and 512 with periodic boundary conditions, using the Swendsen-Wang cluster algorithm [3] in about 5×10^4 measurements at the critical temperature $T_c = 2/\ln(1 + \sqrt{2})$, every τth sweep of the lattice, where τ denotes the autocorrelation time (rounded off to the next largest integer). The value of τ for the various lattice sizes L was estimated from the energy time series to vary from $\tau \approx 4$ for $L = 8$ to $\tau \approx 9$ for $L = 512$. We have chosen the energy time series here as it generally leads to a conservative estimate of the autocorrelation time for cluster algorithms. A total of 5×10^3 lattice sweeps were used for equilibration. Statistical errors were estimated by means of jackknife binning [24].

A. Fractal Dimensions

Tables II, III, IV, and V summarize the values obtained for the critical exponents of the FK and geometrical clus-

ters, as well as of the FK hulls and external perimeters. Where γ/ν and β/ν are listed, both are measured independently by considering the average cluster size χ, which gives γ/ν according to Eq. (3) with $\mathsf{X}(0) = $ const. and the percolation strength P_∞, which gives β/ν according to Eq. (3) with $\mathsf{P}(0) = $ const. The data were fitted using the least-squares Marquardt-Levenberg algorithm.

While including the percolating clusters when considering the mass of the cluster, we ignore them in tracing out cluster *boundaries*. Because of the finite lattice size, large percolating clusters have abnormal small (external) boundaries, so that including them would lead to a distortion of the hull distribution. Moreover, the Grossman-Aharony algorithm [23] we use to trace out the cluster boundaries generally fails on a percolating cluster as its boundary not necessarily forms a single closed loop any longer. With the percolating clusters ignored, the boundary exponents $\beta_{H,EP}/\nu$ cannot be determined, while the summation in the expression (2) for the average cluster boundary size is restricted to nonpercolating clusters.

1. FK Clusters

In Ref. [18], the value $D_C^{FK} = 1.87(1)$ compared to the exact result [19] $D_C^{FK} = 15/8 = 1.875$ was reported for the fractal dimension of FK clusters. It was obtained on a single, but very large lattice ($L = 2^{12} = 4096$) with both open and periodic boundary conditions by considering the number of bond clusters as a function of the radius of gyration. The authors observed a slow and complex approach to the asymptotic behavior and therefore included corrections to scaling to arrive at their numerical estimates. To limit the number of fit parameters, they scanned the fractal dimensions in the neighborhood of the predicted values, and completely fixed the values of the correction exponents to the theoretically predicted ones. This left them with still four parameters to fit. Error bars on the values of the fractal dimensions were determined as the range where $\chi^2/\text{d.o.f.} < 2$.

In this study, where we use different lattice sizes and consider not the bonds, but the sites in a cluster, we find a simple approach to the asymptotic behavior with very small corrections to scaling in the observables required to determine D_C^{FK} all the way down to the smallest lattice considered ($L = 8$). We can therefore apply finite-size scaling without correction terms. Since the fits involve only two parameters, no exponents need to be fixed beforehand. To minimize the effect of unavoidable (small) corrections to scaling, we pick the fit over the largest lattice sizes given in Table II, i.e., over the range $64 - 512$, leading to

$$D_C^{FK} = 1.8753(6) \tag{13}$$

with $\chi^2/\text{d.o.f} = 0.61$ from the average cluster-size data and

$$D_C^{FK} = 1.8752(8) \tag{14}$$

Fit Interval	$\gamma_{\mathrm{C}}^{\mathrm{FK}}/\nu$	$\chi^2/\mathrm{d.o.f.}$	$\beta_{\mathrm{C}}^{\mathrm{FK}}/\nu$	$\chi^2/\mathrm{d.o.f.}$
$8-256$	1.7512(6)	0.89	0.1244(4)	0.74
$16-256$	1.7507(8)	1.02	0.1246(5)	0.95
$32-256$	1.7500(12)	1.39	0.1249(8)	1.31
$40-256$	1.7507(13)	1.43	0.1246(9)	1.43
$64-256$	1.7496(21)	0.52	0.1254(14)	0.33
$8-512$	1.7511(4)	0.86	0.1244(3)	0.71
$16-512$	1.7507(6)	0.95	0.1246(4)	0.88
$32-512$	1.7505(8)	1.23	0.1247(5)	1.14
$40-512$	1.7509(9)	1.20	0.1245(6)	1.17
$64-512$	1.7505(12)	0.61	0.1248(8)	0.47
exact	$1.7500 = 7/4$		$0.1250 = 1/8$	

TABLE II: FK clusters.

with $\chi^2/\mathrm{d.o.f} = 0.47$ from the percolation-strength data. Both estimates are well within one standard deviation from the exact prediction [19] $D_{\mathrm{C}}^{\mathrm{FK}} = 15/8 = 1.875$.

A possible explanation for the improved accuracy we achieved over Ref. [18], although working on smaller lattices, may be that in that study clusters touching the boundary were ignored in the measurements. This set includes all the percolating clusters. As will be illustrated in the next subsection, omitting percolating clusters can lead to strong corrections to scaling.

2. Geometrical Clusters

In Ref. [17], the values $\gamma_{\mathrm{C}}^{\mathrm{G}}/\nu = 1.901(11)$ and $\beta_{\mathrm{C}}^{\mathrm{G}}/\nu = 0.052(2)$ were reported for geometrical clusters. These results were obtained on lattices ranging in size from $L = 600$ to 2000, i.e., again much larger than the ones considered by us. Instead of using periodic boundary conditions, as we did, free boundary conditions were adopted. Another difference from our approach is that percolating clusters were excluded in Ref. [17].

Our estimates, obtained from the largest lattice sizes listed in Table III, i.e., from the interval $64-512$, are

$$D_{\mathrm{C}}^{\mathrm{G}} = 1.9476(3) \tag{15}$$

with $\chi^2/\mathrm{d.o.f} = 0.44$ from the average cluster-size data and

$$D_{\mathrm{C}}^{\mathrm{G}} = 1.9473(4) \tag{16}$$

with $\chi^2/\mathrm{d.o.f} = 0.23$ from the percolation-strength data. Both are in excellent agreement with the exact prediction [7] $D_{\mathrm{C}}^{\mathrm{G}} = 187/96 = 1.9479\ldots$.

In Fig. 2 we show our data for the average cluster size obtained by including all clusters and compare it with the data obtained with percolating clusters excluded from the
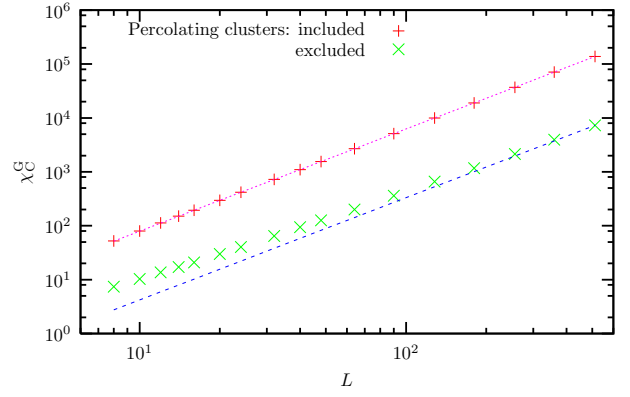

FIG. 2: (Color online) Log-log plot of the average size $\chi_{\mathrm{C}}^{\mathrm{G}}$ of critical geometrical clusters as a function of the lattice size L. Statistical error bars are smaller than the symbol size in the figure. The straight lines proportional to $L^{91/48}$ are put through the data points at $L = 512$ by hand to demonstrate the corrections to scaling for smaller lattice sizes when percolating clusters are excluded, and the absence thereof when they are included in the measurements.

Fit Interval	$\gamma_{\mathrm{C}}^{\mathrm{G}}/\nu$	$\chi^2/\mathrm{d.o.f.}$	$\beta_{\mathrm{C}}^{\mathrm{G}}/\nu$	$\chi^2/\mathrm{d.o.f.}$
$8-256$	1.8941(3)	1.16	0.0532(2)	0.83
$16-256$	1.8944(4)	1.39	0.0530(3)	0.94
$32-256$	1.8946(5)	1.90	0.0528(4)	1.24
$40-256$	1.8950(6)	1.78	0.0526(4)	1.09
$64-256$	1.8949(9)	0.47	0.0527(7)	0.18
$8-512$	1.8943(2)	1.29	0.0531(2)	0.89
$16-512$	1.8946(3)	1.34	0.0529(2)	0.88
$32-512$	1.8949(4)	1.60	0.0528(3)	1.02
$40-512$	1.8951(4)	1.39	0.0526(3)	0.86
$64-512$	1.8951(5)	0.44	0.0527(4)	0.23
exact	$1.8958 = 91/48$		$0.0521 = 5/96$	

TABLE III: Geometrical clusters.

measurements, similarly to what was done in Ref. [17]. While virtually absent in the former, corrections to scaling are present in the latter case. This may explain why, although working on smaller lattices, we obtained much better estimates than in Ref. [17]. We found similar corrections to scaling when instead of percolating clusters, the largest cluster in each measurement was excluded, as is common in random percolation [22].

3. FK Hulls

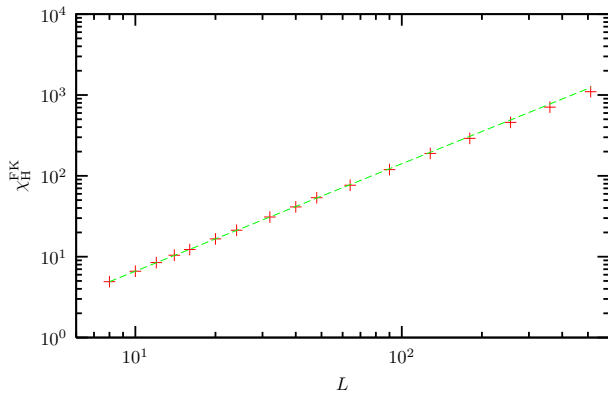Surprisingly, the results for the hulls of FK clusters given in Table IV show a clear tendency to the predicted

FIG. 3: (Color online) Log-log plot of the average hull size χ_H^{FK} of critical FK clusters as a function of the lattice size L. Statistical error bars are smaller than the symbol size in the figure. The straight line $0.310\,L^{1.329}$ is obtained through a two-parameter fit in the interval $8-48$.

value [13] $\gamma_H^{FK}/\nu = 4/3$, corresponding to $D_H^{FK} = 5/3 = 1.6666\ldots$, when restricting the fitting window to increasingly *smaller* lattice sizes. For example, for the interval $8-48$ we find

$$D_H^{FK} = 1.665(3) \tag{17}$$

with $\chi^2/\text{d.o.f} = 0.79$, indicating a good fit. This estimate, which should be compared with the estimate $1.66(1)$ given in Ref. [18], is within one standard deviation from the exact prediction. From Fig. 3 we see that the average FK hull size measured on larger lattices falls below the expected value extrapolated from smaller lattices. We have not been able to determine the cause of this behavior. In fact, when fitting not at the low end but at the high end of the lattice sizes considered, we obtain fits of comparable quality, but the estimate for the exponent converges to a value significantly below the predicted one (see top part of Table IV).

4. Geometrical Hulls

As for the clusters' mass when disregarding percolating clusters, we observe strong corrections to scaling for the hulls of geometrical clusters (see Fig. 4). This is different from what we found using the plaquette update to directly simulate the hulls of the spins on the dual lattice [9], where these corrections were virtually absent (see Fig. 11 of that paper), allowing us to obtain precise estimates for the critical exponents on relatively small lattices. In that study, the largest hull was omitted in each measurement.

To understand the strong corrections to scaling found here for the geometrical hulls, we depict in Fig. 5 the geometrical cluster and the corresponding hull distributions for $L = 32$ normalized to the volume L^2. The bump at the tail of the cluster distribution is due to the finite

Fit Interval	γ_H^{FK}/ν	$\chi^2/\text{d.o.f.}$
$8-512$	1.304(2)	4.71
$16-512$	1.298(2)	3.65
$32-512$	1.288(3)	1.57
$40-512$	1.285(4)	1.36
$64-512$	1.281(5)	0.62
$8-256$	1.311(2)	2.88
$8-128$	1.318(3)	1.50
$8-\ 90$	1.321(3)	1.29
$8-\ 64$	1.325(4)	1.10
$8-\ 48$	1.329(5)	0.79
exact	$1.333 = 4/3$	

TABLE IV: Hulls of FK clusters.

Fit Interval	γ_{EP}^{FK}/ν	$\chi^2/\text{d.o.f.}$
$24-256$	0.763(3)	4.32
$32-256$	0.758(3)	3.10
$40-256$	0.755(4)	3.24
$64-256$	0.748(6)	4.13
$24-512$	0.752(2)	7.97
$32-512$	0.747(2)	5.73
$40-512$	0.744(3)	5.29
$64-512$	0.736(4)	4.37
exact	$0.750 = 3/4$	

TABLE V: External perimeters of FK clusters.

size of the lattice, with percolating clusters gulping up smaller ones reached by crossing lattice boundaries. The subsequent sharp drop-off arises because of the limited number of lattice sites available.

Initially, as Fig. 5 clearly shows, the hull distribution follows more or less the cluster distribution. This is a common feature of all boundary distributions considered. The relatively early drop-off of the hull distribution is because we omit percolating clusters when tracing out cluster boundaries. As a result, the average hull size is underestimated and the data points in Fig. 4 are below the expected line extrapolated from larger lattice sizes. With increasing lattice size, the effect becomes smaller (see Fig. 5, where also the distributions for $L = 512$ are included) and the data points approach the expected asymptotic scaling, corresponding to [20] $\gamma_H^G/\nu = 3/4$, and $D_H^G = 11/8$. Figure 5 shows in addition that the asymptotic behavior of the hull distribution sets in for relatively large hull sizes ($n \gtrsim 100$). On smaller lattices, the asymptotic behavior can therefore simply not
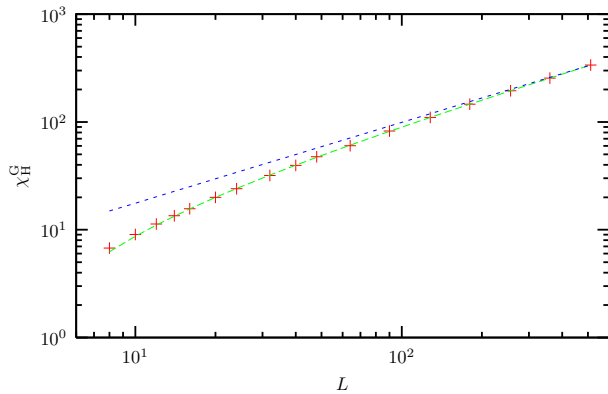
FIG. 4: (Color online) Log-log plot of the average hull size $\chi_{\mathrm{H}}^{\mathrm{G}}$ of critical geometrical clusters as a function of the lattice size L. Statistical error bars are smaller than the symbol size in the figure. The straight line proportional $L^{3/4}$ is put through the data point at $L = 512$ by hand to demonstrate the strong corrections to scaling for smaller lattice sizes. A three-parameter fit in the interval $16 - 512$ gives the value $w = 0.54(3)$ for the effective correction-to-scaling exponent.

be probed, explaining the strong corrections in Fig. 4.

To see if our data are at least consistent with the theoretical prediction, we account for corrections to scaling by fitting the average hull-size data to the form

$$\chi_{\mathrm{H}}^{\mathrm{G}} = a L^{\gamma_{\mathrm{H}}^{\mathrm{G}}/\nu} \left(1 - b L^{-w}\right), \qquad (18)$$

with an effective correction-to-scaling exponent w. We fix $\gamma_{\mathrm{H}}^{\mathrm{G}}/\nu = 3/4$ to the predicted value, leaving us with three parameters (w and the two amplitudes a and b) to fit. For the interval $16 - 512$ we obtain

$$w = 0.54(3) \qquad (19)$$

with $\chi^2/\mathrm{d.o.f} = 1.60$, indicating a reasonable fit (see Fig. 4) and therefore consistency with the theoretical prediction for $D_{\mathrm{H}}^{\mathrm{G}}$.

5. FK External Perimeters

The corrections to scaling are less pronounced for the external perimeters of FK clusters as they are generally smaller than geometrical clusters and thus less likely to percolate (see Fig. 6). Also the asymptotic behavior is reached earlier than for geometrical hulls. The smallness of the corrections allows us to obtain reasonable fits for the average external perimeter size. Our result obtained from the fitting interval $64 - 512$ in Table V yields the fractal dimension

$$D_{\mathrm{EP}}^{\mathrm{FK}} = 1.368(2) \qquad (20)$$

with $\chi^2/\mathrm{d.o.f} = 4.37$. This estimate is compatible with the exact prediction [21] $D_{\mathrm{EP}}^{\mathrm{FK}} = 11/8 = 1.375$, and improves the estimate $D_{\mathrm{EP}}^{\mathrm{FK}} = 1.36(2)$ reported in Ref. [18] by about one order of magnitude.
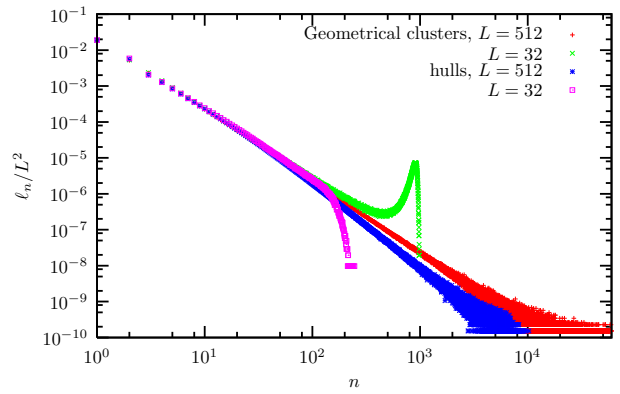

FIG. 5: (Color online) Log-log plot of the (normalized) geometrical cluster and hull distributions at T_{c} on the largest lattice considered ($L = 512$) and on a relatively small lattice ($L = 32$). The number of measurements taken on the largest lattice was about 5×10^4 as in most part of this paper. Statistical error bars are omitted from the data points for clarity. On the smaller lattice, about 5×10^5 measurements, which is an order of magnitude more than used in the rest of the paper, were taken to achieve good statistics. Here, the statistical error bars are smaller than the symbol size in the figure.
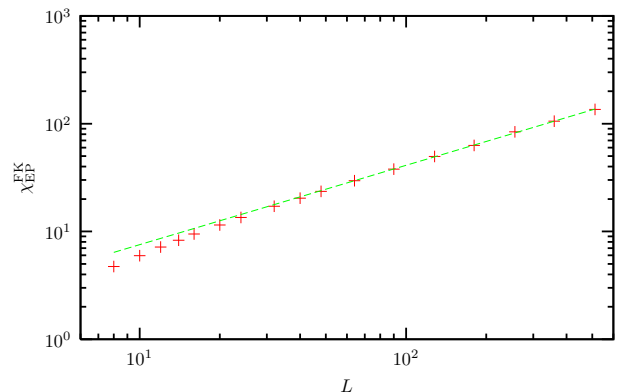

FIG. 6: (Color online) Log-log plot of the average external perimeter size $\chi_{\mathrm{EP}}^{\mathrm{FK}}$ of FK clusters at T_{c} as a function of the lattice size L. Statistical error bars are smaller than the symbol size in the figure. The straight line $1.388\,L^{0.736}$ is obtained through a two-parameter fit in the interval $64 - 512$. Note the corrections to scaling for smaller lattice sizes.

B. Distributions

In Fig. 7, the distributions of the three different boundaries studied are plotted for $L = 512$ to show the crossover of the external perimeters of FK clusters. Starting similarly to the FK hull distribution, the FK external perimeter distribution asymptotically approaches that of the geometrical hulls, in accordance with relation (12). In other words, the FK external perimeter distribution interpolates between that of the FK (for small n) and
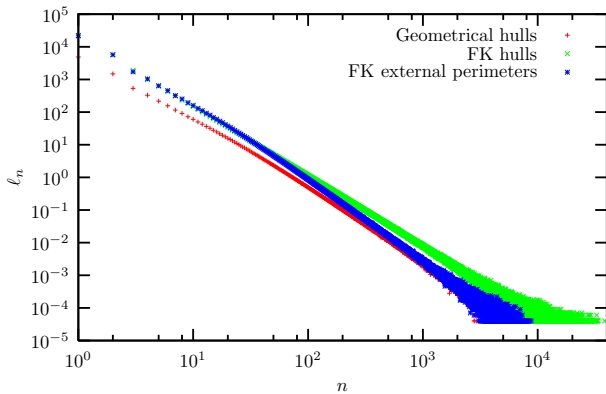
FIG. 7: (Color online) Log-log plot of the distributions of the three different boundaries at T_c for $L = 512$. Statistical error bars are omitted from the data points for clarity. The FK external perimeter distribution initially follows the FK hull distribution before at around $n \approx 100$ it crosses over to its asymptotic behavior which it shares with the geometrical hulls.

geometrical hulls (asymptotically for large n).

Figure 8 summarizes all the cluster and boundary distributions studied for $L = 16$ and 512. The distributions are normalized to the volume L^2. Upon increasing the lattice size, the normalized distributions tend to a universal curve. The slow approach to the asymptotic form of the geometrical hull distribution (and to a lesser extent that of the FK external perimeter distribution), with the associated strong corrections to scaling we observed for these objects, stands out clearly from the other distributions.

It is tempting to directly analyze the distributions ℓ_n and to extract the exponent τ from the asymptotic behavior of ℓ_n, which is algebraic at criticality. However, this method gives far less accurate results than applying finite-size scaling to observables involving the sum $\sum_n$ over the cluster sizes n. The main drawback of the method is the great sensitivity to the location of the fitting window, i.e., the interval of n. The fitting range cannot be started at too small cluster sizes, where the distribution has not taken on its asymptotic form yet, while too large cluster sizes, which are generated only a few times during a complete Monte Carlo run, are also to be excluded because of the noise in the data and finite size effects. Even in those cases for which we obtained very accurate results through finite-size scaling analyses, the direct analysis of the distributions gave unsatisfactory results.

IV. CONCLUSIONS

In this paper, the fractal dimensions of spin clusters and their boundaries appearing in the critical 2D Ising model were studied numerically. The Monte Carlo simulations were carried out on comparatively small lattices. Standard finite-size scaling was applied to obtain very precise estimates for the cluster dimensions, significantly improving existing ones. The results confirm the exact theoretical predictions to a high degree of precision.

For the boundary dimensions, although improving existing estimates, we obtained less accurate results because of corrections to scaling. We observed the strongest corrections for the geometrical hulls, whose distribution approaches its asymptotic form very slowly. In a previous numerical investigation [9], where we simulated the hulls of the spins on the dual lattice directly, corrections to scaling were virtually absent, allowing us to establish the geometrical hull dimension to fairly high precision.

To our surprise, we found the fractal dimension of the FK hulls to converge to the predicted value only when restricting the fitting window to increasingly smaller lattice sizes. In general, one expects of course such a convergence when increasing the lattice size, rather than decreasing it, so as to minimize corrections to scaling. The measured average FK hull size on larger lattices falls below the line extrapolated from smaller lattices. The cause for this behavior eludes us.

To verify relation (12), involving the two different boundary types that can be defined for a cluster, viz. hulls and external perimeters, we treated the two boundary types in a similar manner. Usually, hulls are traced out by a directed random walker on the cluster whereas external perimeters are traced out by a directed random walker probing the cluster from the outside. We, on the other hand, applied the hull algorithm also to the external perimeters of FK clusters, with the proviso that the random walker can move to a nearest neighbor site on the FK boundary even when the connecting bond is not set (for the hull, the bond must be set).
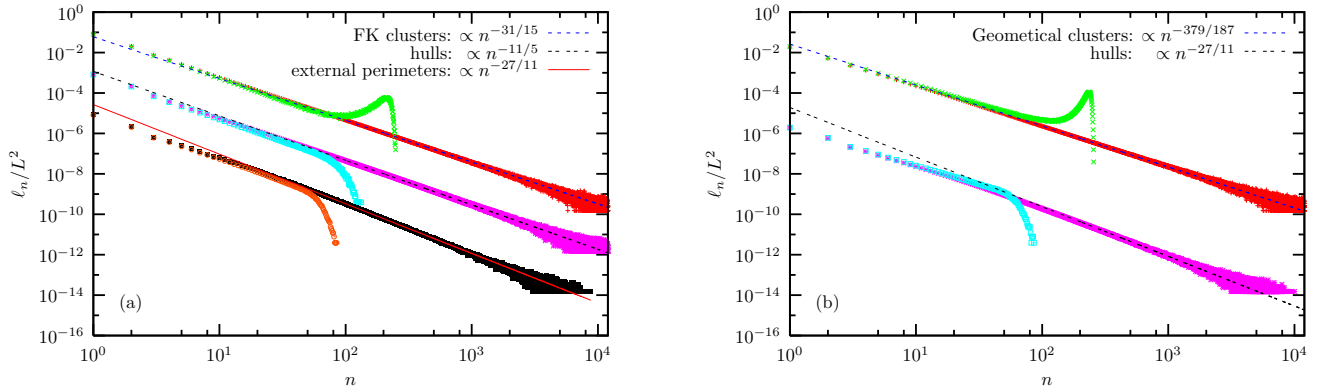
FIG. 8: (Color online) Log-log plot of the critical distributions studied for $L = 16$ (short curves) and 512 (long curves). (a) The (normalized) distributions of FK clusters and of their hulls and external perimeters. For clarity, the latter two are shifted downward by two decades each. (b) The (normalized) distributions of geometrical clusters and of their hulls. The latter is shifted downward by four decades. Statistical error bars are also for clarity omitted from the data points. The straight lines are obtained through one-parameter fits with the slopes fixed to the predicted values. To achieve good statistics for the $L = 16$ lattice, about 5×10^5 measurements were taken–an order of magnitude more than used for the $L = 512$ lattice.

[1] D. Stauffer and A. Aharony, *Introduction to Percolation Theory*, 2nd ed. (Taylor & Francis, London, 1994).
[2] C. M. Fortuin and P. W. Kasteleyn, Physica **57**, 536 (1972).
[3] R. H. Swendsen and J. S. Wang, Phys. Rev. Lett. **58**, 86 (1987).
[4] U. Wolff, Phys. Rev. Lett. **62**, 361 (1989).
[5] B. Nienhuis, A. N. Berker, E. K. Riedel, and M. Schick, Phys. Rev. Lett. **43**, 737 (1979).
[6] J. L. Cardy, M. Nauenberg, and D. J. Scalapino, Phys. Rev. B **22**, 2560 (1980).
[7] A. L. Stella and C. Vanderzande, Phys. Rev. Lett. **62**, 1067 (1989).
[8] C. Vanderzande, J. Phys. A **25**, L75 (1992).
[9] W. Janke and A. M. J. Schakel, Nucl. Phys. B [FS] **700**, 385 (2004).
[10] O. Schramm, *Isr. J. Math.* **118**, 221 (2000).
[11] M. P. M. den Nijs, J. Phys. A **12**, 1857 (1979); Phys. Rev. B **27**, 1674 (1983).
[12] B. Nienhuis, in *Phase Transitions and Critical Phenomena*, edited by C. Domb and J. L. Lebowitz (Academic, London, 1987), Vol. 11, p. 1.
[13] H. Saleur and B. Duplantier, Phys. Rev. Lett. **58**, 2325 (1987).
[14] J. Cardy, in *Phase Transitions and Critical Phenomena*, edited by C. Domb and J. L. Lebowitz (Academic, London, 1987), Vol. 11, p. 55.
[15] B. Duplantier, J. Stat. Phys. **110**, 691 (2003); *Conformal fractal geometry and boundary quantum gravity*, `math-ph/0303034` (2003).
[16] R. Peierls, Proc. Cambridge Philos. Soc. **32**, 477 (1936).
[17] S. Fortunato, Phys. Rev. B **66**, 054107 (2002).
[18] J. Asikainen, A. Aharony, B. B. Mandelbrot, E. M. Rauch, and J.-P. Hovi, Eur. Phys. J. B **34**, 479 (2003).
[19] H. E. Stanley, J. Phys. A **10**, L211 (1977).
[20] C. Vanderzande and A. L. Stella, J. Phys. A **22**, L445 (1989).
[21] B. Duplantier, Phys. Rev. Lett. **84**, 1363 (2000).
[22] K. Binder and D. W. Heermann, *Monte Carlo Simulation in Statistical Physics* (Springer, Berlin, 1997).
[23] T. Grossman and A. Aharony, J. Phys. A **19**, L745 (1986).
[24] B. Efron and R. J. Tibshirani, *An Introduction to the Bootstrap* (Chapman and Hall/CRC, New York, 1998).